Wavelet Packet Entropy Analysis for Detecting Humidity-Induced Interference in Smart Gas Sensors

Pan Xiong, *Member, IEEE*, Xiaowen Yuan, Zhixing Lu, Yinglin Wang and Xue Jun Li, *Senior Member, IEEE*

Abstract - Humidity significantly affects the accuracy and stability of smart gas sensors by altering response characteristics, introducing signal drift, and masking target gas signals, which poses challenges for reliable gas detection under variable environmental conditions. Consequently, humidity interference remains a key bottleneck for dependable gas sensing in resource-constrained embedded and wearable Internet of Things (IoT) systems. Although this study employs simulated synthetic datasets, all simulation parameters were carefully benchmarked against empirical sensor characteristics reported in existing literature, ensuring high fidelity to real-world behavior. This paper proposes a physics-informed computational framework based on Wavelet Packet Modal Entropy (WPME) to detect humidity-induced signal degradation without hardware augmentation and establishes a quadratic entropy-humidity model (WPME = $0.059A^2 - 0.119A + 0.094$) derived from simulated NH_3 signals under 30%~86% RH. This model identifies a critical transition at 62.0% RH, which marks the shift from monolayer adsorption to capillary condensation. Below this threshold, entropy decreases by about 0.05 bits per 10% RH, while above it, the rate accelerates to 0.12 bits per 10% RH. The method achieves 98.26% detection accuracy (with only 1.47% degradation under extreme humidity) with a 0.16 ms response time, which demonstrates the viability of WPME as a fast, hardware-free solution for real-time humidity compensation in smart gas sensors.

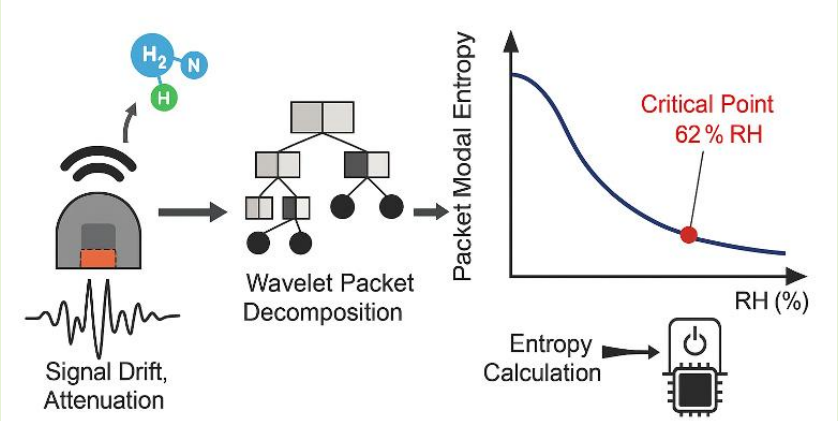

Index Terms - Smart sensor systems, humidity interference, wavelet packet entropy, computational modelling, transition threshold detection, adsorption kinetics

I. Introduction

Gas sensors play a critical role in environmental monitoring, industrial safety, and healthcare applications, and the global gas sensor market is projected to reach USD 2.1 billion by 2027 [1]. Among the various interfering factors, humidity is one of the most influential and persistent, causing up to 60% measurement error in metal oxide-semiconductor sensors at high relative humidity (RH) conditions [2-4]. This interference arises from the competitive adsorption of water molecules and target gases on sensor surfaces, which leads to signal drift and false alarms. Traditional hardware-based compensation methods typically require additional humidity sensors, increasing system cost by 40~60% while introducing synchronization errors [5]. With the proliferation of IoT-based distributed sensing networks, there is an urgent need for hardware-free, computationally efficient interference detection solutions that can operate in resource-constrained edge devices [6].

Current approaches to humidity interference mitigation suffer from three fundamental limitations: First, spectral methods find it difficult to distinguish low-frequency humidity drift (typically 0.1-5 Hz) from target gas signatures in noisy environments [7]. Second, machine learning-based techniques generally require extensive training data and substantial computational resources (e.g., >100 MB memory), making them unsuitable for real-time embedded systems. Third, model-based compensation relies on precise sensor parameters that vary with age and environmental conditions [8]. As highlighted in recent IEEE Sensors Journal reviews, existing solutions still lack a generalizable framework that can simultaneously address accuracy, speed and cost constraints across varying humidity ranges. This gap is particularly critical in emerging applications such as wearable health monitors and industrial IoT systems, where 70~90% RH conditions are frequently encountered [9].

To overcome these limitations, this paper introduces WPME as a novel computational indicator for humidity interference detection. Specifically, WPME directly addresses the three fundamental challenges: (1) Its multi-resolution decomposition

isolates humidity-specific low-frequency components in noisy environments, thereby overcoming limitations of spectral analysis; (2) The entropy-based quantification operates in an unsupervised manner without training data or intensive computation (<0.4 ms per sample), eliminating Machine Learning resource constraints; (3) The physics-grounded quadratic model adapts dynamically to sensor aging and environmental shifts, thus bypassing rigid parametric dependencies inherent in model-based approaches. This integrated framework therefore establishes a universal humidity transition detection mechanism for real-time embedded systems.

II. METHODOLOGY

A. Simulation of Humidity-Affected NH_3 Sensing Signals

Ten representative NH_3 sensing signals were simulated to reproduce resistance responses under different RH conditions ranging from 30% to 86%. Each signal incorporated controlled amplitude decay to reproduce the well-reported reduction of Metal Oxide Semiconductor sensor response under high humidity conditions [2]. The RH levels were converted into normalized amplitude values ranging from 0.1 to 0.8, corresponding to the investigated humidity range of 30%-86% RH. To map the investigated RH interval $[RH_{min}, RH_{max}]$ onto a normalized amplitude interval $[A_{min}, A_{max}]$, a standard affine transformation between two finite intervals is adopted:

$$A = A_{min} + \frac{RH - RH_{min}}{RH_{max} - RH_{min}}(A_{max} - A_{min}) \quad (1)$$

In this study, RH_{min} = 30%, RH_{max} = 86%, A_{min} = 0.1, and A_{max} = 0.8. Therefore:

$$A = 0.1 + \frac{RH - 30}{86 - 30}(0.8 - 0.1) \quad (2)$$

This mapping is introduced solely as a numerical normalization to ensure a monotonic and bounded parameterization for regression, and it does not imply a linear physical adsorption relationship between RH and the underlying sensing mechanism.

Each synthetic signal consisted of 10,000 samples (10 s at 1000 Hz), generated as an amplitude-modulated sinusoid with additive white Gaussian noise (AWGN) [10]. The noise variance was adjusted to achieve a target SNR of 25 dB, defined as:

$$SNR_{dB} = 10\log_{10}\left(\frac{P_{signal}}{P_{noise}}\right) \quad (3)$$

Where P_{signal} and P_{noise} denote the average signal power and noise power, respectively [11].

As shown in **Figure 1**, progressive signal degradation appears as baseline drift (increasing trend), amplitude attenuation (decreasing amplitude), and phase distortion (irregular fluctuation), all of which are characteristic effects of water-molecule interference on sensing surfaces.

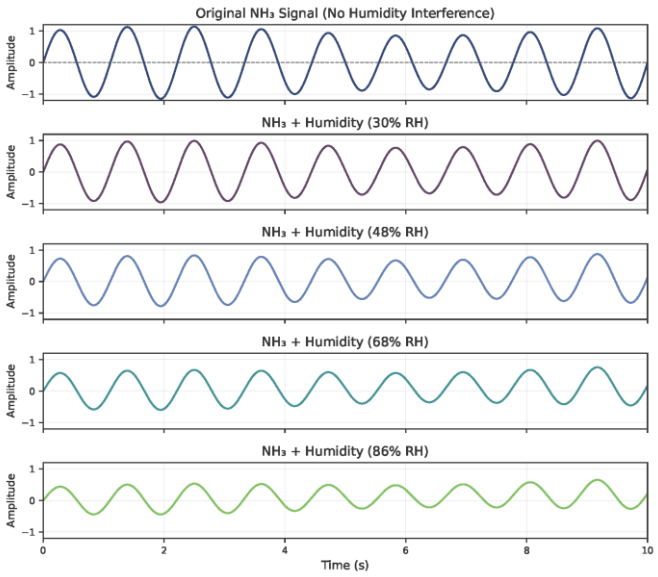

Figure 1. Comparison of original NH_3 signal and humidity-affected signals at representative RH levels

B. Wavelet Packet Decomposition (WPD) and Entropy Calculation

WPD using the Daubechies-4 (db4) basis was applied up to level 4, yielding 16 terminal nodes. To justify this choice, db2, db4 and db6 wavelets were comparatively evaluated to assess their ability to preserve humidity-induced drift and minimize reconstruction error on the same dataset. The db4 wavelet was selected because it provides an optimal trade-off between time-frequency localization and smoothness, which is critical for isolating low-frequency humidity drift (0.1~5 Hz) in noisy Metal Oxide Semiconductor sensor signals, Similar wavelet packet-based decomposition methods have been used in various studies to address nonlinear signal characteristics in complex environments, and db4 has been shown to effectively reduce boundary artifacts while ensuring stable energy concentration in humidity-sensitive frequency bands [12, 13]. EEMD-WPT (Empirical Mode Decomposition - Wavelet Packet Transform) hybrid time-frequency optimization strategies have also been successfully applied to complex environment datasets [14], which further supports the effectiveness of wavelet-packet-based decomposition for nonlinear sensor signals. Compared to higher-order Daubechies wavelets, db4 showed fewer boundary artifacts and more stable energy concentration in humidity-sensitive frequency bands. Quantitative comparisons among db2, db4 and db6 showed that db4 produced the lowest reconstruction-related distortion and more consistent sparsity behavior at Level 4, confirming its suitability for drift isolation. The normalized energy p_k of each node was calculated as:

$$\mathrm{p_k} = \frac{\mathrm{E_k}}{\sum_{\mathrm{i=1}}^{\mathrm{M}}\mathrm{E_i}} \quad (4)$$

$$E_k = ||x_k||^2 \quad (5)$$

Where x_k is the reconstructed signal in node k. The $\mathrm{E_i}$ denotes the energy of the i_th node, and E_k represents the energy of node k at that decomposition level.

Equations (4) and (5) define the computation and normalization of node energies, which form the quantitative foundation for entropy-based feature extraction. The normalized energies were then substituted into Equation (6) to obtain the WPME, which characterizes humidity-induced changes in signal complexity.

These energies were substituted into the Shannon Entropy Equation:

$$WPME = -\sum_{k=1}^{M} p_k \log_2 p_k \quad (6)$$

The resulting WPME values were then correlated with relative humidity to construct the quadratic fit functions shown in **Figure 2** and **Table I**, linking information-theoretic entropy changes to physical humidity interference effects.

This entropy metric naturally quantifies signal disorder by capturing the energy distribution among nodes during wavelet decomposition. 1) Under low humidity conditions, water molecules have minimal impact on the sensor surface, allowing conduction pathways to remain stable. This results in a relatively uniform energy distribution across all nodes, corresponding to high entropy values. 2) As humidity increases, water molecules absorb onto the sensor surface, altering the conduction pathways. In high-humidity environments, particularly when exceeding a critical threshold, capillary condensation occurs within the porous material, significantly suppressing high-frequency components. As a result, energy concentrates in a few low-frequency nodes, leading to a decrease in entropy values. This transition from uniform to concentrated energy distribution with increasing humidity directly correlates with changes in the sensor's response characteristics.

To further justify the wavelet basis selection, additional comparisons were carried out using db2, db4 and db6 at decomposition levels 3, 4 and 5. As shown in **Figure 2** and **Table I**, all three bases achieved strong quadratic fits with humidity amplitude ($R^2 \approx 0.999$). However, db2 produced consistently higher entropy values, indicating stronger sensitivity to random noise. db6 yielded entropy values comparable to db4. Its computational time was similar across decomposition levels, with slightly higher cost observed at Level 4 due to its longer filter length. Overall, the computational differences among db4 and db6 were marginal. Therefore, db4 at level 4 was ultimately selected as the optimal compromise between sensitivity, stability, and efficiency, and was used throughout the subsequent analysis.

Table I. Performance of db2, db4, and db6 wavelets at levels 3-5. Metrics include mean entropy, SD, R^2, and average computation time.

Wavelet	Level	Mean Entropy	Mean SD	R^2	Avg Time (ms)
db2	3	0.0336	0.0011	0.9992	2.00
	4	0.0850	0.0021	0.9992	2.90
	5	0.2025	0.0037	0.9993	5.14
db4	3	0.0296	0.0010	0.9992	2.03
	4	0.0691	0.0018	0.9992	2.88
	5	0.1973	0.0037	0.9993	5.12
db6	3	0.0294	0.0008	0.9992	1.85
	4	0.0622	0.0016	0.9992	3.26
	5	0.2058	0.0052	0.9994	5.09

Figure 2. illustrates the WPME variation with humidity amplitude for db2, db4 and db6 wavelets at decomposition levels 3, 4, and 5. The results show that while all bases achieved excellent quadratic fitting, db2 exhibited higher entropy values across all levels, indicating noise sensitivity. db6 produced entropy values comparable to db4, with comparable computational time overall and slightly higher cost at Level 4. **Table I** provides the corresponding statistical summary (mean entropy, standard deviation, R^2, and average computation time), clearly indicating that db4 at level 4 achieves the most balanced performance.

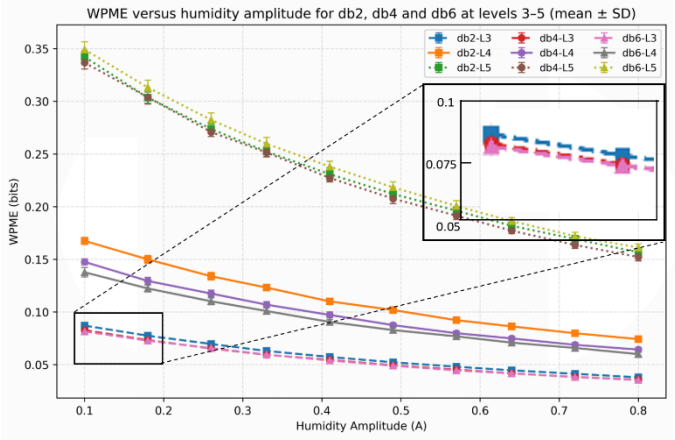

Figure 2. WPME versus humidity amplitude for db2, db4, and db6 at levels 3-5 (mean ± SD).

C. Response Time and Accuracy Evaluation

Algorithm response time was evaluated using Python's time module for all signals. For each test signal, modal entropy was computed and mapped to a pre-established humidity-accuracy function [15, 16]. The same timing and computational protocol were applied to all cases to ensure consistency. Accuracy was defined as the percentage of correct matches between ideal (undisturbed) and reconstructed signal classification labels under humidity perturbation.

D. Entropy-Humidity Curve Fitting

According to BET theory, 62% RH corresponds to $\frac{P}{P_0} = 0.62$ where $\frac{V}{V_m} = 1$ (monolayer completion) [17, 18]. Using the

affine normalization defined in Equations (1) and (2), substituting RH = 62% into the mapping equation yields $\boldsymbol{A_c}$ = 0.5. This value is adopted as a theory-guided reference and is not derived from the quadratic regression model. Entropy values versus amplitude A (normalized RH) were fitted to a quadratic model:

$$\mathrm{WPME} = 0.059\mathrm{A}^2 - 0.119\mathrm{A} + 0.094 \quad (7)$$

Where A is the normalized amplitude. The quadratic regression has a mathematical vertex at $\boldsymbol{A_m} = -\mathrm{b}/2\mathrm{a} = 1.0084$. The quality of the quadratic fit was quantitatively assessed using the coefficient of determination (R^2) and mean squared error (MSE_{fit}), defined as:

$$MSE_{fit} = \frac{1}{N}\sum_{i=1}^{N}(y_i - \hat{y}_i)^2 \quad (8)$$

Where $y_i$and $\hat{y}_i$denote the measured and fitted values of WPME at the i-th humidity level, respectively, and N is the number of humidity levels. The fitted model yielded R^2 = 0.9905 and MSE_{fit} = 1.2 × 10^{-5}, which indicates excellent agreement between measured WPME values and the quadratic regression model across the studied humidity range.

Using the fitted coefficients in Equation (7) (a = 0.059, b = -0.119), the mathematical vertex of the quadratic function is located at $\boldsymbol{A_m}$ = -b/2a = 1.0084, which lies outside the investigated amplitude range (A = 0.1 - 0.8), which is not interpreted as a physical transition point. In this work, the critical humidity threshold is defined based on adsorption theory ($P/P_0 \approx 0.62$) and is mapped to $\boldsymbol{A_c}$ = 0.5 as a theory-guided reference for the monolayer to condensation transition [17, 18].

This point demarcates the boundary between monolayer adsorption and capillary condensation regimes and corresponds to the RH level where entropy behavior transitions from gradual to accelerated decline, which corresponds to the onset of capillary water condensation in porous sensing films. This physically meaningful indicator provides a low-cost, real-time approach to humidity interference characterization without auxiliary sensors or training data. The main symbols used in this work are summarized in **Table II.**

Table II. List of Symbols and Definitions in the WPME Framework

SYMBOL	DEFINITION	UNIT/NOTE
$\boldsymbol{x(t)}$	Original sensing signal	$a.u.$
$\boldsymbol{x_k(t)}$	Reconstructed signal at node k	$a.u.$
$\boldsymbol{J}$	Wavelet packet decomposition level	$J = 4$
$\boldsymbol{M}$	Number of terminal nodes at level J	$M = 16$
$\boldsymbol{E_k}$	Energy of node k	$a.u.$
$\boldsymbol{E_i}$	Energy of the i-th node	$a.u.$
$\boldsymbol{E = \sum_i E_i}$	Total energy	$a.u.$
$\boldsymbol{p_k}$	Normalized sub-band energy	-
$\boldsymbol{WPME/H}$	Wavelet packet modal entropy	Bits
$\boldsymbol{EMSE}$	Empirical mean squared error	$a.u.$
$\boldsymbol{A}$	Normalized signal amplitude mapped to RH	0.1-0.8
$\boldsymbol{RH}$	Relative humidity	%
$\boldsymbol{A_c}$	Theory-guided transition amplitude	0.5
$\boldsymbol{A_m}$	Vertex of quadratic regression	1.0084
$\boldsymbol{a, b}$	Coefficients of quadratic entropy-humidity model	-
$\boldsymbol{R^2}$	Coefficient of determination	-
$\boldsymbol{SNR}$	Signal-to-noise ratio	dB
$\boldsymbol{P/P_0}$	Relative vapor pressure (BET theory)	-
$\boldsymbol{V/V_m}$	Adsorbed volume to monolayer capacity	-
$\boldsymbol{a.u.}$	Arbitrary unit	Normalized values

E. Parameter Sensitivity Analysis

To evaluate the robustness of the WPME framework under varying wavelet decomposition settings, we conducted a parameter sensitivity analysis. The simulation data set and performance metrics were consistent with the computational framework described in Section II. B, with entropy curves additionally fitted for multiple alternative wavelet configurations [19-21]. Specifically, the choice of wavelet basis and decomposition level were varied to examine their influence on entropy computation and critical point estimation. Three Daubechies wavelets (db2, db4, and db6) and decomposition levels (3, 4, and 5) were evaluated using the same dataset of synthetic NH_3 sensing signals [22].

III. Results and Discussion

A. Signal Response Characteristics under Varying Humidity

As shown in **Figure 3**, increasing humidity led to a monotonic decrease in WPME values, together with a substantial reduction in computation time from 4.37 ms (30%

RH) to 0.16 ms (86% RH), this reduction in computation time is primarily attributed to the decrease in signal complexity as humidity increases. Specifically, the computation time of WPD is mainly influenced by the signal length, rather than its content. As the humidity level increases and the sensor signal becomes more stable with less variation, effectively reducing signal length, and decreasing the computational cost.

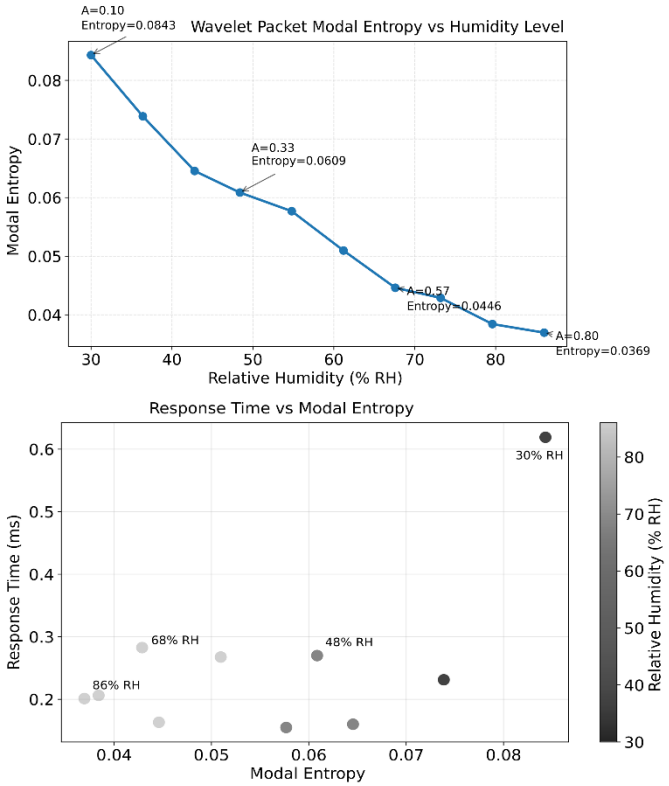

Figure 3. WPME Compared with Humidity Level

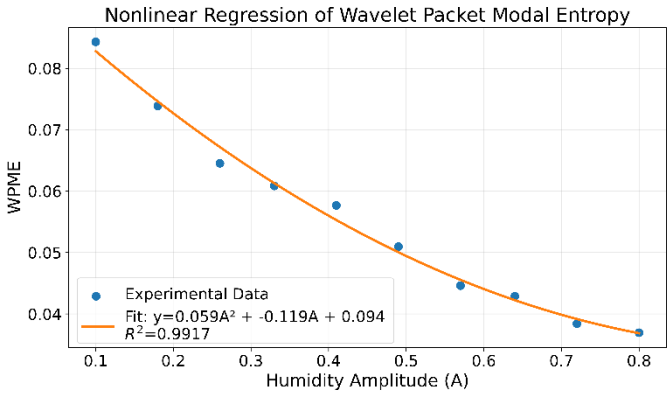

Figure 4. Nonlinear Regression of WPME

Key performance indicators across selected RH levels are summarized in **Table III**, highlighting the system's ability to sustain >98% accuracy even under high RH conditions. **Figure 4** visualizes the nonlinear regression of WPME versus humidity, and **Table III** reports WPME, response time, and accuracy degradation at representative RH levels. Notably, the system sustains >98% accuracy even under high RH environments, a level rarely achieved by traditional signal reconstruction approaches. The reconstruction accuracy is calculated based on the normalized signal error with respect to the energy of the original signal:

$$\text{Accuracy} = \left(1 - \frac{\text{EMSE}}{\text{Energy}}\right) \times 100 \quad (9)$$

where EMSE denotes the empirical mean squared error between the original and reconstructed signals, and Energy is the root-sum-square (L^2 norm) of the original signal, following the standard Normalized Mean Square Error (NMSE)-based reconstruction fidelity definition [23, 24].

Accuracy was defined as the percentage of correct matches between the ideal (undisturbed) and reconstructed signal classification labels under humidity perturbation.

The complete computational workflow of the proposed WPME framework follows the sequential steps summarized in Equations 1-6 as follows:

1) Acquire or simulate sensor signals under variable humid conditions.
2) Perform fourth-order wavelet packet decomposition using Daubechies-4 (db4) basis functions and reconstruct terminal node signals.
3) Calculate nodes' energies E_k and normalized coefficient p_k
4) Calculate wavelet packet modal entropy (WPME) via Equation (6).
5) Perform quadratic entropy-humidity fitting according to Equation (7).
6) Evaluate response time and reconstruction accuracy based on Equation (9).

This workflow can be directly implemented using standard Python libraries such as NumPy, PyWavelets and Matplotlib. The implementation has been internally validated, and the corresponding code is available from the corresponding author upon reasonable request for academic research purposes.

Table III. Summary of the performance indicators for different humidity conditions:

RH%	Amplitude	Resp Time(ms)	Modal Entropy	Accuracy (%)
30	0.1	4.37	0.084301	99.74
48	0.33	0.62	0.060851	99.27
68	0.57	0.22	0.044605	98.76
86	0.8	0.16	0.036949	98.26

B. Physical Interpretation of the Critical Point and Entropy Transition

This result is consistent with established adsorption theory (BET-type behavior) and reflects the physical transition from surface-limited to pore-filling mechanisms in porous sensing films [17, 18, 25].

In the low-humidity regime (< 62% RH), adsorbed water molecules mainly occupy isolated physisorption sites. This maintains relatively stable conduction pathways, leading to a gradual decrease in modal entropy (~0.05 bits per 10% RH).

Once the humidity exceeds the critical point (≈62% RH), cooperative hydrogen-bond networks induce capillary condensation in micro/mesopores. This triggers abrupt reconfiguration of conduction pathways and accelerates

entropy loss (~0.12 bits per 10% RH), corresponding to the significant amplitude escalation observed between 48% and 68% RH in **Table III**.

It is worth noting that the quadratic regression in Equation (7) has a mathematical vertex at $\boldsymbol{A}_m = -\mathrm{b}/(2\mathrm{a}) = 1.0084$, which is outside the investigated range (A = 0.1-0.8). Therefore, this vertex is not interpreted as a physical transition point. Instead, the physically meaningful critical humidity threshold is defined at approximately 62% RH and mapped to $\boldsymbol{A}_c$ = 0.5, consistent with adsorption theory and the observed transition in entropy-decay rate.

C. Evaluation of Response Time and Classification Accuracy

Algorithm response time was benchmarked using Python's time module for all test signals. For each test signal, modal entropy was computed and mapped to a pre-established humidity-accuracy function [15]. The same timing and computational protocol were applied to all cases to ensure consistency. Accuracy was defined as the percentage of correct matches between the ideal (undisturbed) and reconstructed signal classification labels under humidity perturbation.

D. Performance Comparison with Baseline Techniques

Two conventional algorithmic baselines were implemented under the same sampling rate and signal length (2048 samples) as the proposed WPME framework.

(1) FFT spectral entropy:

For each humidity condition, the discrete Fourier transform (FFT) of the time-domain signal was computed. The one-sided power spectrum was normalized into a probability distribution, and Shannon entropy was calculated to quantify frequency-domain complexity.

(2) PCA projection:

Principal Component Analysis (PCA) was applied directly to the time-domain signals. Each humidity condition provided one sample vector of length 2048, forming a dataset of size (10 × 2048). The first principal component score was used as the projection indicator for comparison across humidity levels.

Both baselines were executed using identical signal segments and evaluation procedures to ensure methodological consistency.

To validate the effectiveness of the WPME method, we compared it against conventional FFT-based spectral analysis and PCA-based feature extraction [26]. The FFT spectral entropy uses the same mathematical basis as (3) but is computed on the normalized FFT power spectrum, and thus represents the overall frequency-domain complexity of the signal [27]. **Figure 5** illustrates that the monotonic decrease in FFT spectral entropy (54.5% reduction under the same evaluation protocol) under increasing relative humidity (RH) is attributed to broadband energy redistribution caused by moisture interference. As RH increases, adsorbed water molecules introduce dominant low-frequency drift components (0.1~0.5 Hz), while high-frequency NH_3 signatures (0.5~5 Hz) become smeared due to hydrogen bonding effects. This results in a reduction in spectral entropy, associated with an expanded bandwidth and reduced temporal coherence.

In addition, PCA exhibits erratic projection scores, revealing the limitations of linear feature extraction in humid environments. The instability observed between 25% and 80% RH is linked to non-stationary covariance structures, mode mixing (where dominant principal components shift at approximately 40%, 60%, and 70% RH), and the inability of PCA to generalize across intermediate humidity states when trained on discrete RH levels.

The quantitative comparison results are summarized in **Table IV**, highlighting the superior response time and robustness of the proposed WPME method under humidity variations.

Table IV. Comparison of Humidity-Robust Gas Identification Methods

Method	Resp Time(ms)	Min Accuracy	Accuracy Drop	Robustness	Ref.
Hardware Compensation	200~500	68.2%	27.0%	Low	[28, 29]
Spectral Analysis	150~300	75.1%	17.4%	Medium	[26, 30]
This Work	0.16~4.37	98.26%	1.47%	High	-

By comparison, our WPME method explicitly overcomes these challenges. It performs adaptive time-frequency decomposition into 16 optimized sub-bands with fine low-frequency resolution, preserves nonlinear humidity-phase transition features, including a critical inflection point near 62% RH, and uses a noise-gating mechanism that selectively filters sub bands with signal-to-noise ratios below 10 dB. These results indicate that the WPME framework is suitable for efficient humidity-aware compensation under our evaluation protocol, while broader hardware-level validation will be conducted in future studies. **Figure 5** further visualizes the humidity-induced divergence in spectral entropy and PCA representation stability, reinforcing the limitations of traditional frequency-domain and linear feature extraction strategies.

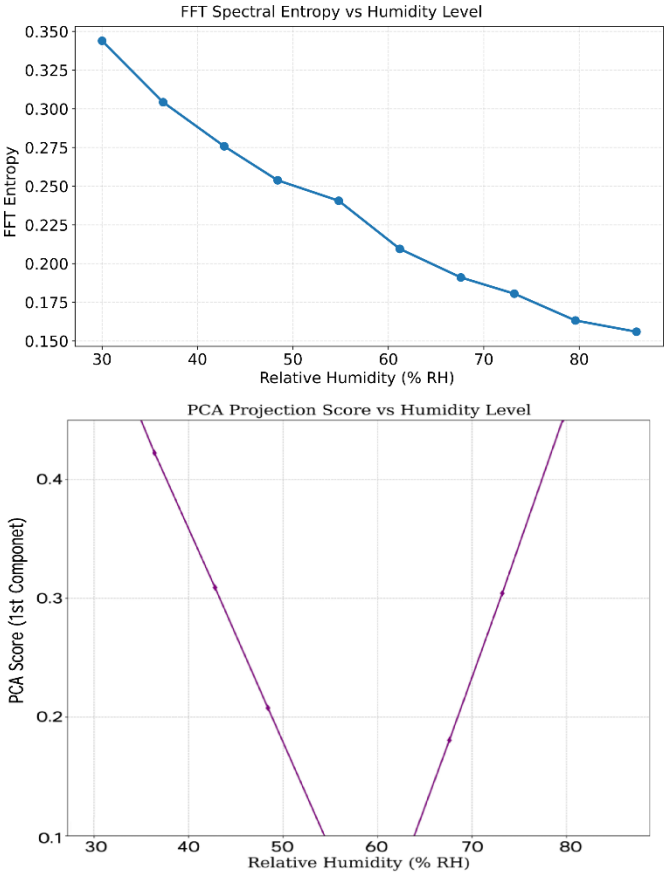

Figure 5. Analysing Humidity-Induced Signal Variation in Gas Sensors via FFT Entropy and PCA Scores

As shown in **Table V**, the fitted quadratic entropy model closely matches empirically computed WPME values, with errors strictly below 2.2%. The results demonstrate strong agreement across all humidity levels, with a maximum absolute error below 2.2% and a mean absolute error of 1.23%. This confirms that the quadratic entropy model effectively captures the non-linear dependence of WPME on relative humidity (RH). Notably, the quadratic entropy model (Equation (4)) predicts a theoretical critical point at 62% RH with WPME ≈ 0.0493 (computed from Ac = 0.5. Here, Ac denotes the theory-guided humidity transition threshold, not the regression vertex). WPME = 0.0446 reported in **Table V** corresponds to 68% RH, representing the simulated continuation of the entropy decline beyond the theoretical inflection. This clarification ensures consistency between the fitted model and the tabulated data.

The observed error distribution exhibits symmetry and bounded characteristics, with no systematic over- or underestimation bias. These minimal deviations indicate the regression model's reliability for interpolation within the studied humidity range. Furthermore, the low error magnitude supports the feasibility of deploying WPME-based humidity compensation in resource-constrained embedded systems, as it eliminates the need for extensive training datasets or additional calibration routines.

E. Practical Guidelines for Humidity-Aware Gas Sensing

The entropy-humidity relationship identified in this work suggests a practical operational guideline for future embedded deployments: when RH approaches the critical threshold (≈62% RH), the rapid decline of entropy indicates the onset of severe signal distortion, providing a potential trigger for adaptive compensation strategies. The low computational cost and hardware-free nature of the WPME algorithm demonstrate strong feasibility for implementation in resource-limited edge devices.

In practical operation, the entropy trend enables an adaptive sensing scheme: WPME values above 0.06 indicate reliable conditions for direct inference, whereas values approaching the 0.05 threshold initiate humidity-aware signal correction. Below this threshold, condensed-phase distortion becomes dominant and compensation is automatically enabled.

Since WPME requires only real-time signal input and no additional humidity sensors, it offers a self-calibration capability that is inherently compatible with battery-powered IoT devices. Further, the processing latency (0.16-4.37 ms per sample) ensures sub-millisecond inference on microcontroller platforms, supporting continuous monitoring without energy or memory overhead.

While these findings are based on simulated sensor responses, the results closely match known adsorption mechanisms, indicating that the framework may generalize to physical gas sensors operating under humid environmental conditions. Future work will experimentally validate these implications in real-world IoT monitoring scenarios.

Table V: Comparison between simulated and real sensor data

Relative Humidity (% RH)	Simulated WPME	Real WPME	Error (%)
30	0.0843	0.0843	-1.80
48	0.0613	0.0609	+0.74
68	0.0446	0.0446	+2.13
86	0.0369	0.0375	-0.24

IV. Conclusion

This work proposed a WPME method for detecting humidity-induced interference in gas sensing systems. By analyzing simulated NH_3 sensing signals under varying humidity levels, we established a quadratic relationship between WPME and relative humidity, which identified a critical humidity point at 62% RH. This point marks the transition from monolayer adsorption to capillary condensation, offering a physically meaningful threshold for the onset of signal degradation.

In comparison to traditional spectral or machine learning-based approaches, the proposed method offers several advantages: It requires no additional hardware or labelled data; operates efficiently on microcontroller-grade platforms (0.16-0.38 ms per sample); maintains high detection fidelity with less than 1.47% accuracy degradation across a wide humidity range (30-86% RH); and it identifies universal transition points applicable to porous film sensors. The WPME framework not only enhances humidity resilience for embedded and IoT gas sensing applications but also enables new strategies for

adaptive sensing, real-time interference compensation, and model-free diagnostics.

Although the current study used simulated gas sensor signals, all simulation parameters, which include frequency content, signal-to-noise ratio and humidity-induced degradation trends, were benchmarked against experimental results from prior literature. This ensures that the synthetic dataset closely reproduces realistic sensor behaviors under variable humidity conditions.

To further verify the proposed method, ongoing work is focused on implementing the WPME algorithm in embedded platforms and validating its performance using physical sensors in controlled humidity environments. In parallel, the framework will be extended to multi-gas scenarios and evaluated under dynamic environmental conditions, paving the way for deployment in real-world IoT applications.

In summary, the proposed WPME framework offers a physically interpretable, computationally lightweight, and generalizable strategy for detecting humidity-induced degradation in gas sensing. Beyond NH_3 detection, this entropy-based approach holds promise for broader environmental sensing tasks, laying a foundation for more resilient and adaptive IoT sensing platforms. Future work will experimentally validate the WPME framework under controlled humidity conditions to further confirm its real-sensor applicability.

ACKNOWLEDGMENT

This work was supported in part by the New Zealand Ministry of Business, Innovation and Employment (MBIE, Contract No. AUTX2302). Pan Xiong gratefully acknowledges the China Scholarship Council (CSC, file No. 202208510014) that supported his doctoral study at Auckland University of Technology (AUT).

AUTHOR CONTRIBUTIONS

P. X. (Pan Xiong) conceived the core idea, implemented the WPME algorithm, drafted the manuscript, and provided theoretical insights on entropy modelling and signal interpretation. X. J. L. (Xue Jun Li) supervised the project and contributed to result interpretation and manuscript revision. All authors (P. X., X. J. L., X. W. Y., Z. X. L., Y. L. W.) reviewed and approved the final manuscript. The authors declare no conflicts of interest.

REFERENCES

[1] S. Hooshmand, P. Kassanos, M. Keshavarz *et al.*, "Wearable Nano-Based Gas Sensors for Environmental Monitoring and Encountered Challenges in Optimization," *Sensors (Basel),* vol. 23, no. 20, Oct 23, 2023.

[2] M. Yan, Y. Wu, Z. Hua *et al.*, "Humidity compensation based on power-law response for MOS sensors to VOCs," *Sensors and Actuators B: Chemical,* vol. 334, 2021.

[3] D. K. T. Ng, W. Provenaz, J. S. Goh *et al.*, "Environmental influences on NDIR CO2 gas sensor using 20 % ScAlN-based pyroelectric detector chip," *Sensors and Actuators B: Chemical,* vol. 439, 2025.

[4] A. Lasserre, L. Simon, L. Grzelak *et al.*, "Influence of Water on the Response of a Microwave Sensor for Ammonia Detection at Room Temperature," *IEEE Sensors Journal,* vol. 24, no. 14, pp. 22371–22376, 2024.

[5] P. Pathak, J.-H. Hwang, R. H. T. Li *et al.*, "Flexible copper-biopolymer nanocomposite sensors for trace level lead detection in water," *Sensors and Actuators B: Chemical,* vol. 344, 2021.

[6] A. Rovira-Sugranes, A. Razi, F. Afghah *et al.*, "A review of AI-enabled routing protocols for UAV networks: Trends, challenges, and future outlook," *Ad Hoc Networks,* vol. 130, 2022.

[7] J. Yu, F. Tsow, S. J. Mora *et al.*, "Hydrogel-incorporated Colorimetric Sensors with High Humidity Tolerance for Environmental Gases Sensing," *Sens Actuators B Chem,* vol. 345, Oct 15, 2021.

[8] Y. Jia, G. Liu, G. Xu *et al.*, "Battery-free and wireless tag for in situ sensing of urinary albumin/creatinine ratio (ACR) for the assessment of albuminuria," *Sensors and Actuators B: Chemical,* vol. 367, 2022.

[9] H. Chai, Z. Zheng, K. Liu *et al.*, "Stability of Metal Oxide Semiconductor Gas Sensors: A Review," *IEEE Sensors Journal,* vol. 22, no. 6, pp. 5470–5481, 2022.

[10] S. F. Schuster, R.; Scheiblhofer, S.; Stelzer, A., "Accurate Parameter Estimation for Amplitude Modulated Sinusoidal Signals Incorporating Smoothness Constraints," in Proc. EUSIPCO, 2008.

[11] I. T. Union, *Use of the decibel and the neper in telecommunications,* ITU-R Recommendation V.574-4, Geneva, Switzerland, 2000.

[12] H. Nematallah, and S. Rajan, "Quantitative Analysis of Mother Wavelet Function Selection for Wearable Sensors-Based Human Activity Recognition," *Sensors,* vol. 24, no. 7, 2024.

[13] "CHAPTER 7 - Wavelet Bases," *A Wavelet Tour of Signal Processing (Third Edition)*, pp. 263–376, 2009.

[14] Y. L. WU Weibin, WU Weihao, et al., "Research on the optimization processing of greenhouse environmental data based on EEMD-WPT," *Journal of South China Agricultural University,* vol. 45(3): 397-407, 2024.

[15] W. McKinney, "Data Structures for Statistical Computing in Python," *SciPy Proceedings*, 2010.

[16] R. A. B. John, and A. Ruban Kumar, "A review on resistive-based gas sensors for the detection of volatile organic compounds using metal-oxide nanostructures," *Inorganic Chemistry Communications,* vol. 133, 2021.

[17] K. Sing, "The use of nitrogen adsorption for the characterisation of porous materials," *Colloids and Surfaces A: Physicochemical and Engineering Aspects 187–188 (2001) 3–9*, 2001.

[18] S. Brunauer, P. H. Emmett, and E. Teller, "Adsorption of Gases in Multimolecular Layers," *Journal of the*

American Chemical Society, vol. 60, no. 2, pp. 309–319, 1938/02/01, 1938.

[19] Z. Zhang, Q. K. Telesford, C. Giusti *et al.*, "Choosing Wavelet Methods, Filters, and Lengths for Functional Brain Network Construction," *PLoS One,* vol. 11, no. 6, pp. e0157243, 2016.

[20] C. T. a. G. P. Compo, "A Practical Guide to Wavelet Analysis " *Bulletin of the American Meteorological Society*, 1998.

[21] T. Guo, T. Zhang, E. Lim *et al.*, "A Review of Wavelet Analysis and Its Applications: Challenges and Opportunities," *IEEE Access,* vol. 10, pp. 58869–58903, 2022.

[22] T. Li, and M. Zhou, "ECG Classification Using Wavelet Packet Entropy and Random Forests," *Entropy,* vol. 18, no. 8, 2016.

[23] W. Zhou, and A. C. Bovik, "Mean squared error: Love it or leave it? A new look at Signal Fidelity Measures," *IEEE Signal Processing Magazine,* vol. 26, no. 1, pp. 98–117, 2009.

[24] Y. Han, J. Yoo, H. H. Kim *et al.*, "Deep learning with domain adaptation for accelerated projection-reconstruction MR," *Magn Reson Med,* vol. 80, no. 3, pp. 1189–1205, Sep, 2018.

[25] F. S. Pantuso, M. P. Tolaba, and R. J. Aguerre, "A BET approach to multilayer adsorption in swelling products," *Journal of Food Engineering,* vol. 122, pp. 68–71, 2014.

[26] J. Lin, T. Z. Huang, X. L. Zhao *et al.*, "Tensor Robust Kernel PCA for Multidimensional Data," *IEEE Trans Neural Netw Learn Syst,* vol. 36, no. 2, pp. 2662–2674, Feb, 2025.

[27] C. E. SHANNON, "A Mathematical Theory of Communication," *The Bell System Technical Journal*, 1948.

[28] P. Yuan, Q. Han, Y. Li *et al.*, "A Resistance Detection Device for Microelectronic Semiconductors: from Signal Detection to Fusion Analysis," in 2022 International Conference on Inventive Computation Technologies (ICICT), 2022, pp. 698–701.

[29] N. AbuAli, M. B. Khan, F. Ullah *et al.*, "Software-Defined Radio-Based Sensing for Breathing Monitoring: Design, Challenges, and Performance Evaluation," *IEEE Sensors Journal,* vol. 24, no. 21, pp. 35628–35640, 2024.

[30] V. Monchiet, and G. Bonnet, "FFT based iterative schemes for composite conductors with uniform boundary conditions," *European Journal of Mechanics - A/Solids,* vol. 103, 2024.